Available online at www.sciencedirect.com
SCIENCE DIRECT®
International Journal of Heat and Mass Transfer 49 (2006) 17–29
International Journal of HEAT and MASS TRANSFER
www.elsevier.com/locate/ijhmt

Single-phase and two-phase cooling with an array of rectangular jets

Michael T. Meyer [a], Issam Mudawar [a,*], Chad. E. Boyack [b], Charles A. Hale [b]

[a] *Purdue University, School of Mechanical Engineering, International Electronic Cooling Alliance, 585 Purdue Mall, West Lafayette, IN 47907, USA*
[b] *Raytheon Missile Systems, Tucson, AZ 85706, USA*

Received 24 May 2005; received in revised form 15 July 2005
Available online 2 November 2005

Abstract

Experiments were performed to explore the effects of jet width, impingement velocity, and inlet subcooling on the cooling performance of an array of three confined rectangular FC-72 and ethanol jets impacting a 3.0 cm × 3.0 cm heated surface. The single-phase heat transfer coefficient increased with increasing jet velocity and/or jet width. A correlation for single-phase cooling was constructed by dividing the flow into impingement zones and confinement channel flow regions that are dominated by wall jet flow. Increases in jet velocity, jet width, and/or subcooling broadened the single-phase region preceding the commencement of boiling and enhanced critical heat flux (CHF). A new correlation was developed which fits the CHF data with good accuracy. Overall, better cooling performance was realized for a given flow rate by decreasing jet width. Pressure drop was for the most part quite modest, even for the smallest jet width and highest velocity tested. Overall, these results prove the present cooling scheme is highly effective at maintaining fairly isothermal surface conditions, with spatial variations of less than 1.2 and 2.6 °C for the single-phase and boiling regions, respectively. These results demonstrate the effectiveness of the present jet-impingement scheme for thermal management of next generation electronics devices and systems.

1. Introduction

Pursuit of faster computing speed during the past four decades has spurred an industry-wide race to micro-miniaturize electronic components and integrate as many components as possible in a single device. These developments have triggered unprecedented increases in heat dissipation from high performance devices.

The need to tackle the escalating heat dissipation has often been an afterthought, left as one of the final design hurdles to overcome using such conventional means as conduction through the device's substrate and convection to ambient air. But as heat dissipation rates kept mounting, designers discovered these conventional means were no longer effective, and had to shift their attention to the use of liquids as coolants. This shift

* Corresponding author. Tel.: +1 765 494 5705; fax: +1 765 494 0539.
E-mail address: mudawar@ecn.purdue.edu (I. Mudawar).

0017-9310/$ - see front matter © 2005 Elsevier Ltd. All rights reserved.
doi:10.1016/j.ijheatmasstransfer.2005.07.039

Nomenclature

a	empirical constant
A_s	area of test surface
b	empirical constant
C	empirical constant
C_1, C_2, C_3	empirical constants
c_p	specific heat at constant pressure
C_{sub}	empirical constant
H	channel height
$\bar{h}_L$	average heat transfer coefficient for test surface
h_{fg}	latent heat of vaporization
k	thermal conductivity
L	length of test surface corresponding to one jet cell
L_h	length of entire test surface
m	empirical constant
n	empirical constant
N	number of jets in array
$\overline{Nu}_L$	average Nusselt number for test surface
p	pressure
Δp	pressure drop
P_e	electrical power input
p_{in}	pressure at test module inlet
p_{out}	pressure at test module outlet
Pr	Prandtl number
q''	heat flux
q''_m	critical heat flux
q^{**}_m	dimensionless critical heat flux
Re	jet Reynolds number, $U(2W)/\nu_f$
Re_c	Reynolds number based on channel velocity
ΔT	temperature difference, $T_s - T_{in}$
T_{in}	fluid temperature at test module inlet
ΔT_{max}	maximum temperature variation along test surface
T_s	average temperature of test surface
T_{sat}	saturation temperature
T_{si}	local test surface temperature above thermocouple *TCi*
ΔT_{sub}	subcooling, $T_{sat} - T_{in}$
T_{tc}	temperature measured by thermocouple *TCi*
U	mean jet velocity
U_c	channel velocity
W	jet width
W_e	total width of exit corresponding to one jet cell

Greek symbols

ρ	density
ν	kinematic viscosity
σ	surface tension

Subscripts

f	saturated liquid
g	saturated vapor
in	test module inlet
out	test module outlet
s	test surface
sat	saturation
sub	subcooling

has yielded substantial improvement in heat removal because of the superior thermophysical properties of liquids.

Liquid jet impingement is one of the most effective means of achieving very high convection coefficients, especially when the coolant undergoes phase change. Choice of jet configuration is based on several practical considerations including operating environment, coolant compatibility, and, of course, heat dissipation and surface temperature. The jet is typically issued normal to the heat-dissipating surface through a circular or a rectangular (slot) orifice. The convection coefficient is highest in the impact zone below the orifice and diminishes away from the impact zone. The average heat transfer coefficient for a large surface can be increased substantially and the surface temperature rendered more uniform by using multiple jets [2]. Another variation of jet-impingement cooling is to confine the path of spent coolant to prevent the chaotic splashing encountered with free jets during vigorous boiling [3–7].

While jets can demand higher coolant flow rates than competing high performance cooling schemes, they do offer significant advantages. For example, compared to micro-channel flow, they facilitate the removal of very high heat fluxes with relatively modest pressure drops. They are also highly adaptable to cooling multiple devices in a compact package [1], ensure temperature uniformity when using multiple confined jets [2], and are applicable to both terrestrial and microgravity environments, as well as can endure the severe body forces induced by military aircraft maneuvers [8].

The present study capitalizes upon the merits of jet impingement in pursuit of a versatile thermal management solution for a broad range of applications. Despite their inferior thermal transport properties compared to water, Fluorinert liquids are especially suited for electronic cooling applications. Aside from superior dielectric properties, these liquids are chemically inert, producing negligible corrosiveness on most metallic surfaces. Furthermore, Fluorinerts come in a broad range

of boiling points. By choosing a coolant which boils 30–40 °C below the maximum allowable surface temperature of the heat-dissipating device, it is possible to capitalize upon the merits of nucleate boiling [1]. Multiple rectangular jets are used in the present study because of their suitability to cooling square or rectangular surfaces, and their ability to more effectively and uniformly expel the spent fluid away from the impingement zone compared to multiple circular jets. Another feature of the present impingement geometry is confinement of the spent fluid with the aid of a jet plate that is placed parallel and in close proximity to the heat-dissipating surface. This flow confinement serves two important purposes, limiting recirculation and combating splashing during boiling. Without confinement, the spent coolant can recirculate, bringing the spent hot fluid to interact again with the heated surface, and degrading cooling effectiveness. Flow confinement also combats splashing of the jet liquid away from the heated surface during vigorous boiling. Caused by vapor momentum perpendicular to the surface, liquid splashing causes gradual reduction of liquid access to the surface and premature dryout farther downstream from the impingement zone [3–7]. A jet plate situated a short distance away from the heated surface serves to maintain liquid in close proximity to the surface even during intense boiling.

2. Experimental methods

2.1. Flow loop

Fig. 1 shows the schematic of the flow loop that was configured to supply Fluorinert FC-72 (or ethanol) to the desired flow rate, pressure and temperature to a jet-impingement test module. The liquid was circulated in the loop with the aid of a variable speed magnetically coupled pump. The liquid was passed through a 5-μm filter, a rotameter, and a fan-cooled subcooler before entering the test module.

Exiting the test module, the two-phase mixture was routed to a reservoir, where liquid was allowed to settle to the bottom while the vapor was released to a condenser situated atop the reservoir, condensed and trickled down to the reservoir. The liquid drained directly into a deaeration chamber situated below the reservoir. Contained within the deaeration chamber was an immersion heater that was used to boil off any air dissolved in the coolant.

2.2. Jet-impingement module

As shown in Fig. 2(a), the primary components of the test module were a heater block, a jet plate, and a plastic

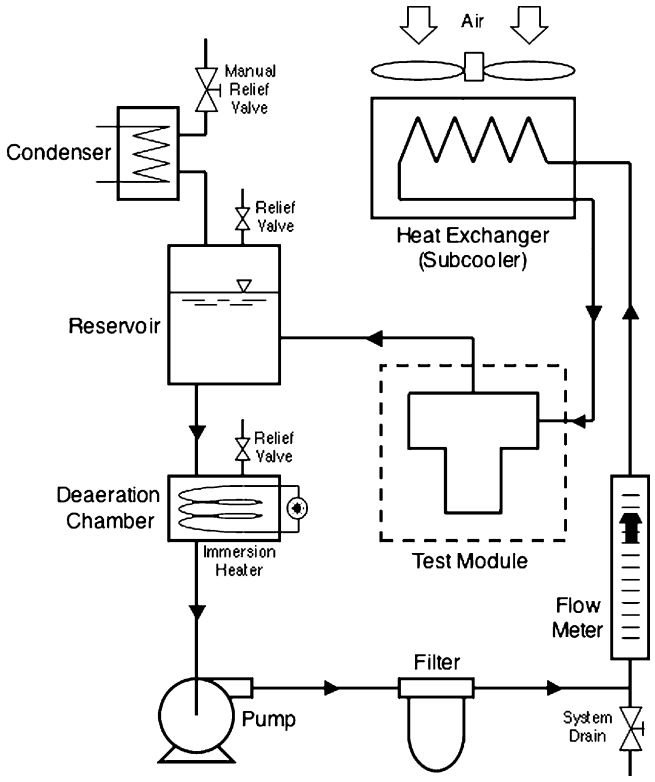

Fig. 1. Schematic of flow loop.

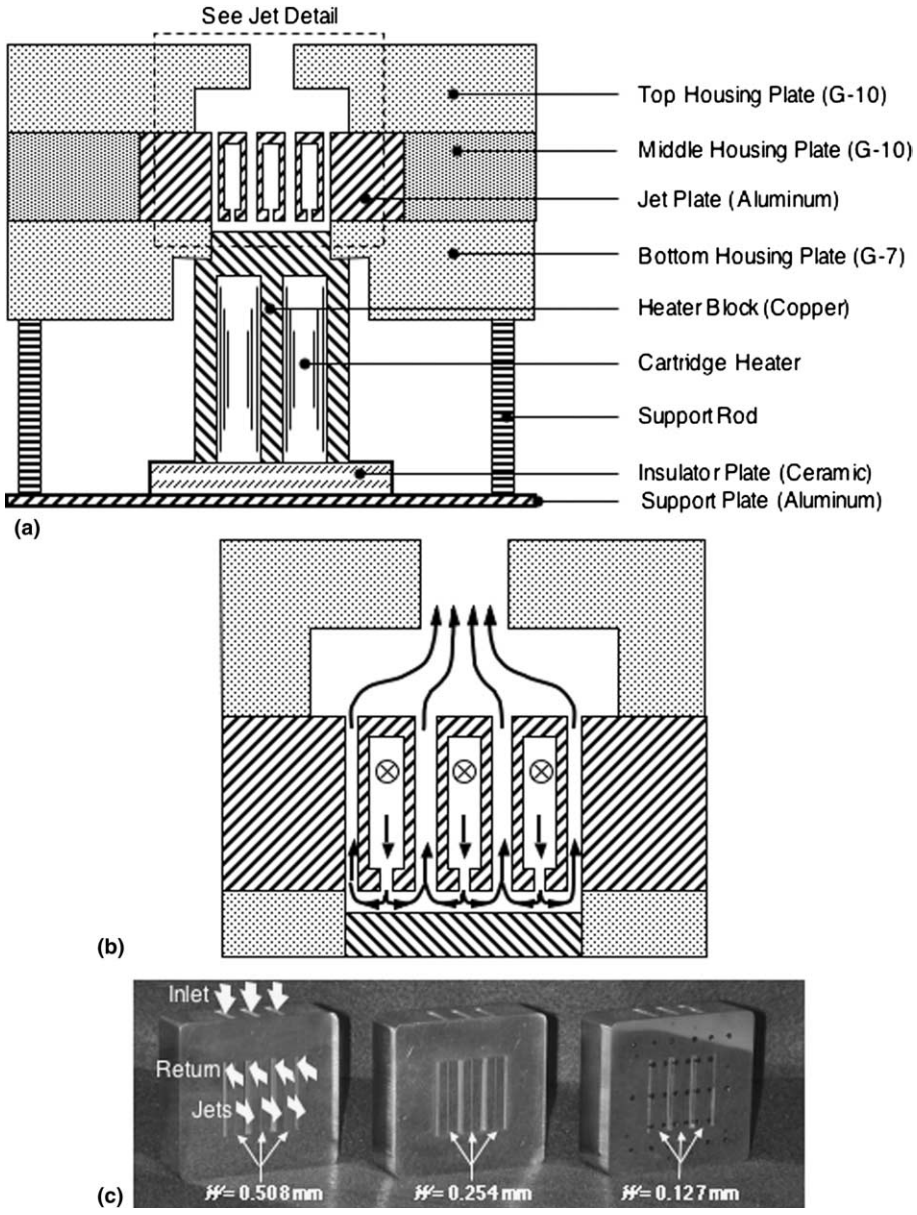

Fig. 2. (a) Construction of test module, (b) coolant path inside module and (c) photos of underside of jet plates.

housing. The entire assembly was held together with the aid of four support rods extending from a support platform. The top surface of the heater block constituted the heat-dissipating 'test surface' impacted by the jets. The three-layer housing served to both hold the jet plate and heater in place and minimize heat loss to the ambient. The top and middle layers were machined from G-10, and the bottom layer from G-7. G-10 and G-7 are fiberglass plastics made from a continuous glass woven fabric base that is impregnated with epoxy resin or silicone binder, respectively. The bottom layer was in direct contact with the heater block and therefore benefited from the higher temperature capability of G-7.

The heater block was made from oxygen free copper. The top $3.0\,\text{cm} \times 3.0\,\text{cm}$ surface of the copper block comprised the test surface of the module subjected to jet impingement. Four high watt density cartridge heaters were inserted into bores machined into the underside of the block.

Fluid leaks were prevented by applying high-temperature RTV silicone rubber along the interfaces between the heater block and the G-7 plate of the housing, and

by Viton O-rings that were inserted between the fiberglass plastic plates.

Three jet slots were machined into each of three aluminum jet plates. The slots were formed by one of two methods. The first consisted of electrical discharge machining (EDM) with graphite electrodes. This method was very effective for jet widths of 0.254 and 0.508 mm, but difficulties arose with the smallest, 0.127 mm, jets. For the latter, the electrodes were quite thin and tended to warp slightly, producing a defective rectangular orifice. A second method was therefore devised for the 0.127 mm jets. It involved breaking the jet plate into several pieces. First, a piece was fabricated that had plenums machined into an aluminum block. Next, four plates with a thickness equivalent to the nozzle height were fabricated and slots for the exits machined into each. A fine grinding wheel was used to remove half the jet thickness from each of two mating plates. The jet plate was made by fastening the pieces together using small machine screws. The screw heads were then ground flush with the jet plate surface.

All three aforementioned jet plates were constructed for the FC-72 tests. A fourth jet plate with a jet width of 1.00 mm was later fabricated to obtain a few CHF data points for ethanol.

The test module employed a compact 3D design that ensured even flow distribution between jets. The coolant was supplied through a port in the back of the middle fiberglass plastic plate, which was followed by a diverging plenum. A deflector plate situated midway along the diverging plenum causes the fluid to stagnate before reaching the jet plate. This helped ensure even flow distribution between jets as opposed to favoring the center jet. The flow was divided among three small plenums in the jet plate, one situated above each jet orifice as shown in Fig. 2(b). The fluid then impinged upon the test surface of the heated copper block, situated 5.60 mm below the orifices. The fluid then flowed horizontally away from the impingement zone and collided with fluid from the neighboring jets or the sidewalls. Above the collision planes were four exit channels that were machined clear through the jet plate. Once the fluid passed through the four exit channels, it rejoined in a plenum above the jet plate before exiting the test module. Fig. 2(c) shows photos of the three jet plates.

Heat flux along the test surface, q'', was determined by dividing the measured electrical power input, P_e, by

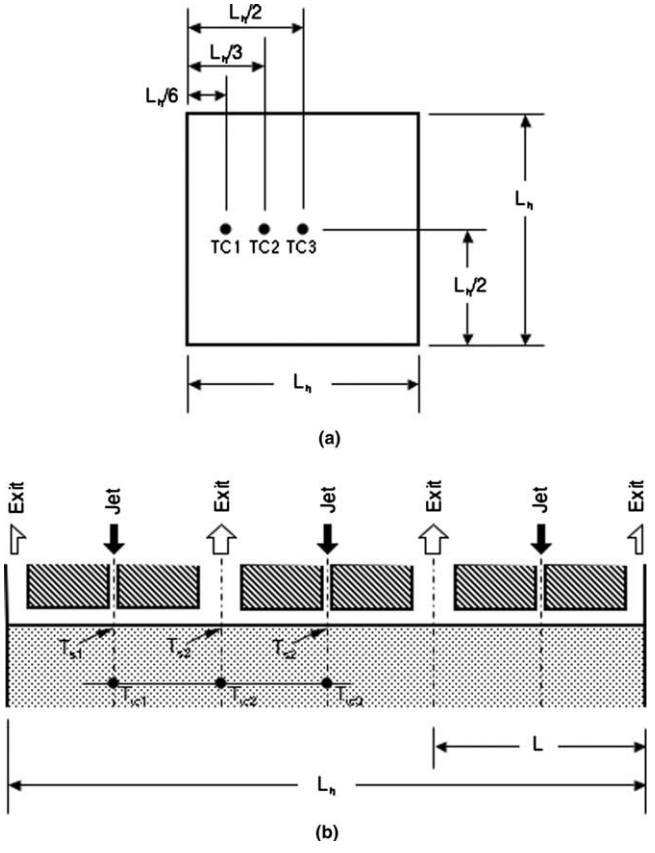

Fig. 3. Thermocouple locations shown in (a) top view and (b) side view of heater block.

the area of the test surface, A_s (9.0 cm^2). This method for determining heat flux assumes zero heat loss to the ambient. The actual heat loss was greatly minimized by using low thermal conductivity insulation around the heater block.

Three type K (Chromel–Alumel) thermocouples were used to monitor the temperature of the test (impingement) surface. The thermocouples were inserted 2.54 mm below the test surface. As shown in Fig. 3(a) and (b), one thermocouple was placed directly beneath the central jet, a second beneath a side jet, and a third beneath the exit between the two jets. The thermocouple measurements were corrected for the temperature gradient across the 2.54 mm copper layer between the thermocouple beads and the test surface. The average test surface temperature, T_s, was determined by averaging the surface temperatures above the three thermocouples.

Thermocouples with exposed beads were used to measure the test module's inlet and outlet fluid temperatures. The module inlet and outlet pressures were measured by pressure transducers connected to pressure taps at the same locations as the flow thermocouples.

2.3. Operating conditions

The jet-impingement module employed an array of three 3.0 cm long rectangular jets to cool the 3.0 cm × 3.0 cm test surface. Each jet provided cooling for an $L = 1.0$ cm wide portion of the test surface. As indicated earlier, three different jet widths ($W = 0.127$, 0.254 and 0.508 mm for FC-72 and $W = 1.00$ mm for ethanol) were examined over a broad range of jet velocities and two levels of subcooling. The jet plate was situated a distance $H = 5.60$ mm above the test surface.

The operating conditions for FC-72 are summarized in Table 1. For each test, FC-72 was conditioned to enter the test module at either 10.6 ± 0.3 or 20.6 ± 0.3 °C subcooling. Pump capacity set upper velocity limits of 3, 5, and 8 m/s for the 0.508, 0.254 and 0.127 mm jet plates, respectively. On the other hand, the flow meter set a lower limit of 1 m/s corresponding to the 0.127 mm jet plate.

It should be emphasized that the present study is focused mostly on the assessment of heat transfer trends for FC-72. A few tests were performed with ethanol for the sole purpose of broadening the application range of the CHF correlation resulting from the present study. These data points are discussed later in this paper.

2.4. Measurement uncertainty

The electrical power input to the heater block was measured by a Yokogawa WT200 power analyzer with 0.5% measurement accuracy. Heat loss from the copper block was estimated at less than 3% of the total heat input. Uncertainties in the pressure transducer, rotameter, and thermocouple measurements were 0.5%, 1.0%, and 0.3 °C, respectively.

3. Experimental results

Fig. 4(a) and (b) shows FC-72 boiling curves for the 0.127 mm jet for 10.6 and 20.6 °C subcooling, respectively. For all 14 tests, the boiling curves exhibit trends that are consistent with those reported in the jet-impingement literature. Single-phase heat transfer prevailed over a fairly broad range of surface temperatures, evidenced by a linear dependence of heat flux on surface-to-fluid temperature difference. Increasing jet velocity increased the single-phase heat transfer coefficient, yielding an upward shift in the heat flux–temperature difference characteristics. Another effect of increasing jet velocity was a broadening of the single-phase region and delayed commencement of nucleate boiling. There was a general tendency of nucleate boiling data for different velocities to converge. Some decay in heat transfer effectiveness occurred before CHF, evidenced by a decline in the slope of the boiling curve from the high values corresponding to the nucleate boiling region. CHF increased monotonically with increasing jet velocity.

Comparing Fig. 4(a) and (b) shows the single-phase region is, for the most part, unaffected by subcooling; any minor differences in this region are the result of fluid property variations with temperature. For a given velocity, the onset of nucleate boiling was significantly delayed by the increase in subcooling. This amounts to a broader

Table 1
Operating conditions for FC-72 experiments

Jet width, W	0.127 mm	0.254 mm	0.508 mm
Inlet subcooling at CHF, ΔT_{sub}	10.6 ± 0.2 °C, 20.6 ± 0.2 °C	10.6 ± 0.2 °C, 20.6 ± 0.2 °C	10.6 ± 0.2 °C, 20.6 ± 0.2 °C
Jet velocity, U	2.0–8.0 m/s	1.0–5.0 m/s	1.0–3.0 m/s
Inlet pressure, p_{in}	$1.09–1.51 \times 10^5$ N/m^2 (15.82–21.96 psi)	$1.06–1.43 \times 10^5$ N/m^2 (15.31–20.68 psi)	$1.11–1.88 \times 10^5$ N/m^2 (16.05–27.25 psi)
Outlet pressure, p_{out}	$1.03–1.09 \times 10^5$ N/m^2 (14.91–15.84 psi)	$1.04–1.14 \times 10^5$ N/m^2 (15.01–16.52 psi)	$1.04–1.18 \times 10^5$ N/m^2 (15.08–17.12 psi)
Saturation temperature, T_{sat} (at p_{out})	57.1–58.9 °C	57.3–60.2 °C	57.4–61.2 °C

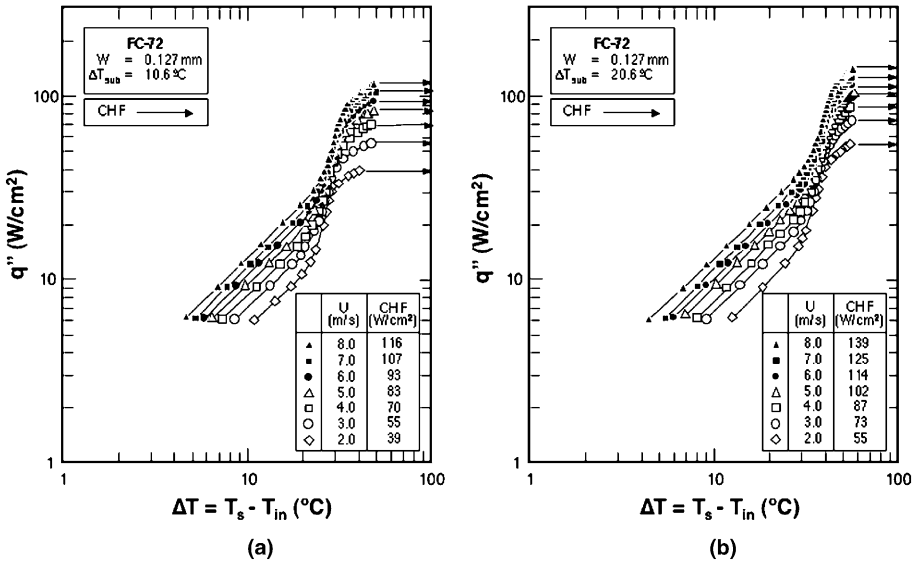

Fig. 4. FC-72 boiling curves for 0.127 mm jet with (a) 10.6 °C subcooling and (b) 20.6 °C subcooling.

single-phase region at the higher subcooling. CHF was significantly enhanced by the higher subcooling.

Fig. 5(a) and (b) shows similar trends for the 0.508 mm jet, however, both the single-phase heat transfer coefficient and CHF are higher than those for the 0.127 mm jet for the same jet velocity.

A key performance parameter for any high-flux electronic cooling scheme is the ability to maintain a fairly isothermal device surface. Surface temperature variations generally increased with increasing heat flux. Remarkably, however, the averages of the single-phase data for $T_{s2} - T_{s1}$ and $T_{s2} - T_{s3}$ (see Fig. 3) over the entire single-phase region were less than 1.2 and 0.9 °C, respectively.

4. Single-phase correlation

The flow geometry adopted in the present jet-impingement study shares several similarities with a previous study by Wadsworth and Mudawar [9,10]. The primary difference between the two configurations is

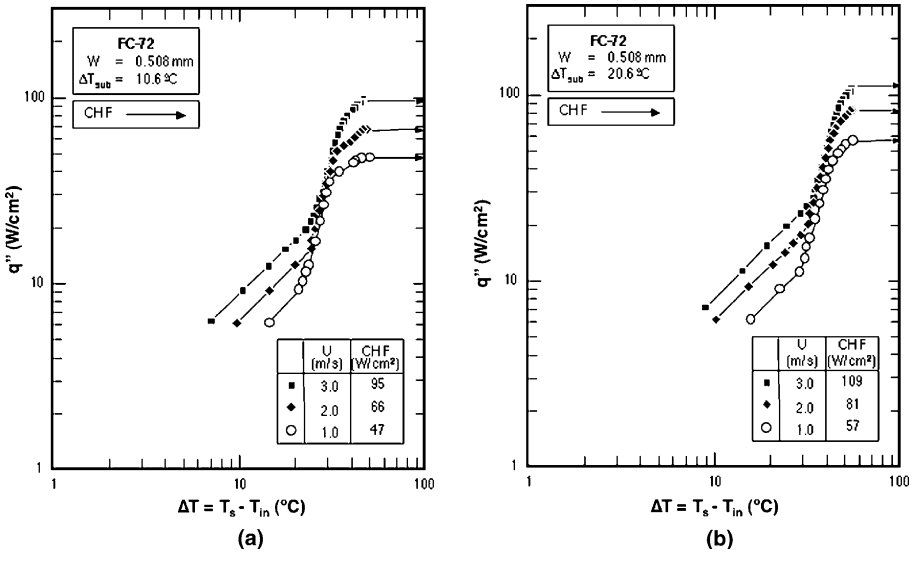

Fig. 5. FC-72 boiling curves for 0.508 mm jet with (a) 10.6 °C subcooling and (b) 20.6 °C subcooling.

related to both multi-jet packaging and means of expelling the fluid from the cooling module. As shown in Fig. 6(a), the Wadsworth and Mudawar configuration involved expelling coolant issued from a single jet laterally in confinement channels into enlarged channels (not shown in Fig. 6) that are perpendicular to the page. The present configuration, on the other hand, employed an array of three interacting jets and included exit channels above the outer edges of the confinement channels.

A new correlation is sought for the single-phase region of the present flow geometry. The test surface is divided into segments representing cells that are each cooled by a single jet. The length of each cell is defined as $L = L_h/N$, where L_h is the total length of the heated surface and N the number of jets or cooling cells.

Using a superposition technique developed by Wadsworth and Mudawar [9], an overall heat transfer correlation is sought by dividing each test cell into two regions, one directly below the impinging jet and a second comprised of the two channel flow regions.

$$\frac{\bar{h}_L L}{k_f}\frac{1}{Pr_f^{1/3}} = \frac{q'' L}{k_f(T_s - T_{in})}\frac{1}{Pr_f^{1/3}} = \frac{\overline{Nu}_L}{Pr_f^{1/3}} = C_1 Re^a + C_2 Re_c^b, \tag{1}$$

where Re is the Reynolds number for a single jet, $U(2W)/\nu_f$, and Re_c the Reynolds number for the channel portions, $U_c(L - W)/\nu_f$.

Eq. (1) introduces an unknown parameter, U_c, which represents channel velocity. One method for determining this parameter is to use mass conservation,

$$U_c = \frac{UW}{2H}. \tag{2}$$

However, Wadsworth and Mudawar proved this velocity yields poor correlation results since their heat transfer data showed virtually no dependence on channel

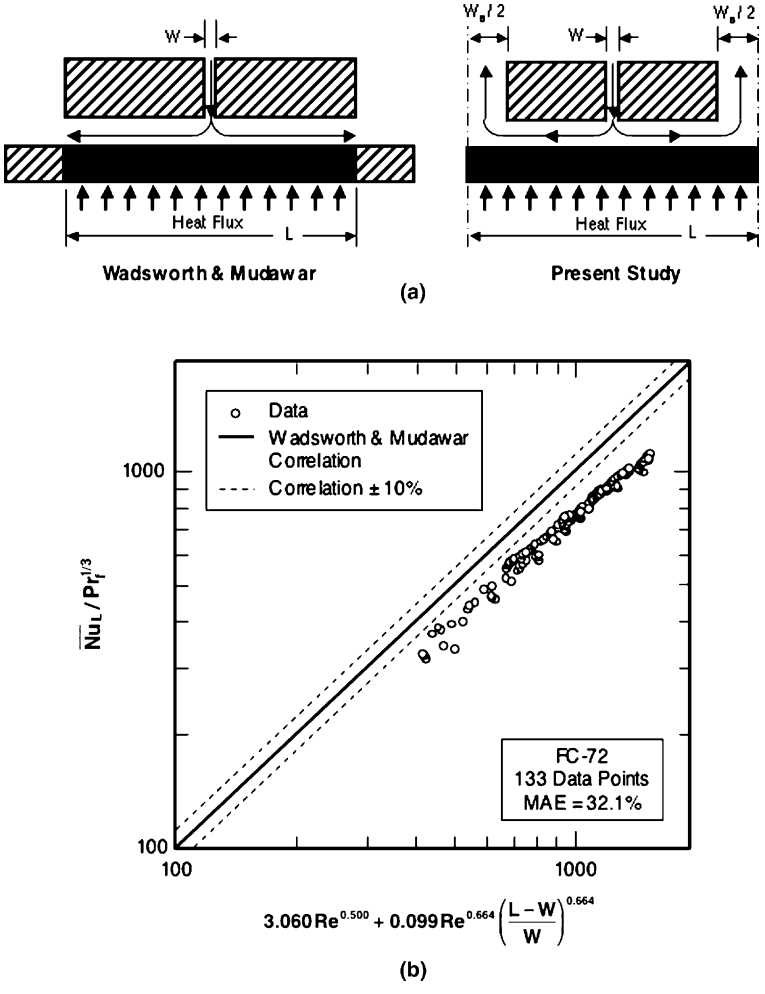

Fig. 6. (a) Comparison of impingement geometry of Wadsworth and Mudawar and one cell of present study and (b) present single-phase FC-72 heat transfer data versus single-phase Wadsworth and Mudawar correlation.

height. They postulated that, excluding impractically small values of H, fluid flow in the lateral channels behaves as a wall jet, whose velocity is approximately equal to the jet velocity,

$$U_c = U. \tag{3}$$

Eq. (1) can therefore be written as

$$\frac{\overline{Nu}_L}{Pr_f^{1/3}} = C_1\left[\frac{U(2W)}{\nu_f}\right]^a + C_2\left[\frac{U(L-W)}{\nu_f}\right]^b, \tag{4}$$

or in terms of the jet Reynolds number,

$$\frac{\overline{Nu}_L}{Pr_f^{1/3}} = C_1 Re^a + C_3 Re^b\left(\frac{L-W}{W}\right)^b, \tag{5}$$

where $C_3 = C_2/2^b$.

Based on prior jet studies, Wadsworth and Mudawar showed the impingement zone can be accurately characterized by setting $a = 0.50$. This technique led to the following correlation:

$$\frac{\overline{Nu}_L}{Pr_f^{1/3}} = 3.060Re^{0.50} + 0.099Re^{0.664}\left(\frac{L-W}{W}\right)^{0.664}, \tag{6}$$

which showed good agreement with their FC-72 data as well as prior data for mass transfer to free gaseous jets [11,12].

Fig. 6(b) shows appreciable deviation of the present FC-72 data from Wadsworth and Mudawar's single jet correlation because of both jet interaction and differences in coolant exit. Using the present database, the following new correlation was derived using the same superposition technique:

$$\frac{\overline{Nu}_L}{Pr_f^{1/3}} = 3.060Re^{0.50} + 0.118Re^{0.694}\left(\frac{L-W}{W}\right)^{0.694}, \tag{7}$$

which is valid for $1400 < Re < 14{,}400$. Fig. 7(a) shows Eq. (7) fits the present FC-72 data with a mean absolute error of 2.96%. Fig. 7(b) shows this correlation is equally successful at fitting data for the three jet widths.

5. CHF results

Fig. 8(a) shows the variation of CHF for FC-72 with jet velocity for different jet widths and subcoolings. On average, increasing the subcooling by 10 °C resulted in an 18 W/cm^2 or 26% increase in CHF. A quick inspection of Fig. 8(a) may lead to the conclusion that a slight increase in velocity should deliver the largest improvement in CHF when using the widest jet. While this is indeed the case, it is important to note that the 0.508 mm jet requires a flow rate four times greater than the 0.127 mm jet for the same jet velocity.

A more insightful way to compare data is to explore the dependence of CHF on flow rate. Fig. 8(b) shows, for a given flow rate, decreasing jet width actually increases CHF. This finding is of paramount practical importance since it proves great improvement in CHF is possible simply by reducing jet width, provided the fluid delivery loop can tackle the increased pressure drop.

Table 2 provides a summary of CHF values and corresponding pressure drops and average surface temperatures for all the present tests. This table shows pressure drop at CHF increases with increasing velocity

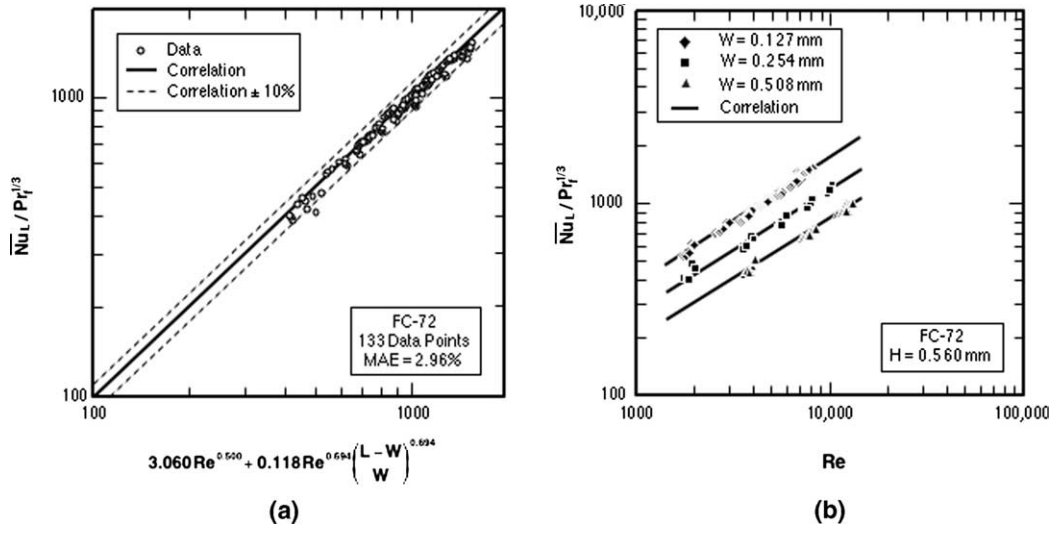

Fig. 7. (a) Correlation of present single-phase FC-72 heat transfer data and (b) comparison of correlation predictions with FC-72 data for individual nozzle widths.

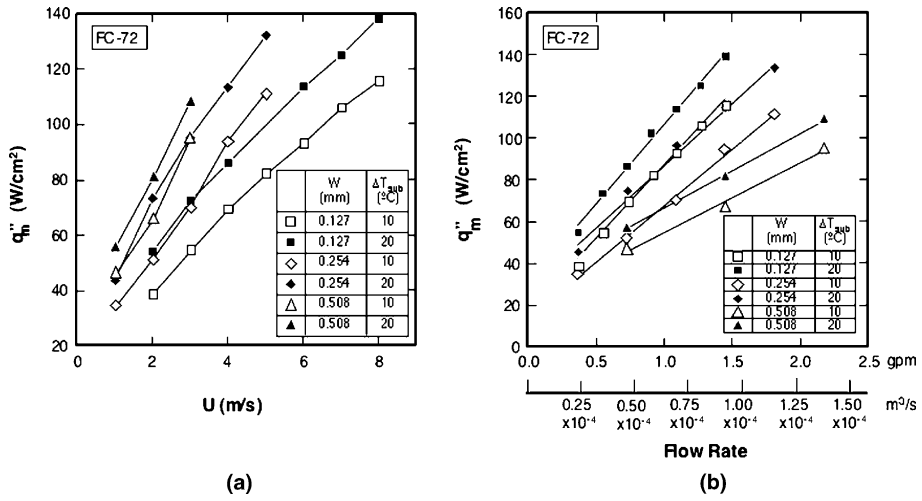

Fig. 8. Variations of CHF for FC-72 with (a) jet velocity and (b) flow rate for different jet widths and subcoolings.

Table 2
Data for pressure drop and mean surface temperature at CHF for FC-72

W (mm)	U (m/s)	$\Delta T_{sub} = 10.6 \pm 0.3$ °C			$\Delta T_{sub} = 20.6 \pm 0.3$ °C		
		q''_m (W/cm^2)	Δp (N/m^2) (psi)	T_s (°C)	q''_m (W/cm^2)	Δp (N/m^2) (psi)	T_s (°C)
0.508	1.0	47.0	5239 (0.76)	95.9	57.0	5102 (0.74)	90.7
	2.0	66.0	13,238 (1.92)	95.4	81.0	9446 (1.37)	92.1
	3.0	95.0	27,716 (4.02)	96.2	109.0	27,923 (4.05)	94.5
0.254	1.0	35.0	2137 (0.31)	90.6	44.0	1999 (0.29)	86.5
	2.0	51.0	5585 (0.81)	87.1	74.0	4895 (0.71)	85.1
	3.0	70.0	11,100 (1.61)	87.8	95.0	10,135 (1.47)	87.3
	4.0	94.0	18,064 (2.62)	91.6	114.0	17,788 (2.58)	88.1
	5.0	111.0	28,751 (4.17)	92.8	132.0	28,751 (4.17)	89.3
0.127	2.0	39.0	7170 (1.04)	87.1	55.0	7446 (1.08)	91.9
	3.0	55.0	13,100 (1.90)	93.4	73.0	14,134 (2.05)	92.5
	4.0	70.0	21,442 (3.11)	93.5	87.0	22,546 (3.27)	91.7
	5.0	83.0	31,922 (4.63)	95.2	102.0	34,887 (5.06)	93.1
	6.0	93.0	44,195 (6.41)	95.5	114.0	47,022 (6.82)	92.4
	7.0	107.0	59,708 (8.66)	97.3	125.0	61,293 (8.89)	92.7
	8.0	116.0	77,358 (11.22)	95.3	139.0	77,703 (11.27)	92.5

and decreasing jet width; the highest pressure drop was encountered with the narrowest jet at the highest velocity. Fig. 9 shows a parabolic dependence of pressure drop at CHF for FC-72 with flow rate for different jet widths and subcoolings. While decreasing jet width increases pressure drop appreciably, the magnitude of pressure drop is for the most part quite modest.

The highest surface temperature, 97.3 °C, was measured with the 0.127 mm jet at 7 m/s and 10.6 °C subcooling. With one exception (0.127 mm, 2 m/s), an increase in subcooling decreased the surface temperature at CHF; the surface temperature was on average 2.8 °C cooler at 20.6 °C subcooling than at 10.6 °C.

5.1. CHF correlation

Mudawar and Wadsworth [10] developed the following CHF correlation for their single jet configuration:

$$\frac{\left[\dfrac{q''_m/(\rho_g h_{fg})}{U}\right]}{\left[\dfrac{\rho_f}{\rho_g}\right]^{2/3}\left[1+\dfrac{c_{pf}\Delta T_{sub}}{h_{fg}}\right]^{1/3}\left[1+C_{sub}\dfrac{\rho_f c_{pf}\Delta T_{sub}}{\rho_g h_{fg}}\right]^{2/3}} = C\left[\frac{\sigma}{\rho_f U^2(L-W)}\right]^m\left[\frac{W}{L-W}\right]^n, \quad (8)$$

where $C_{sub} = 0.058$, $C = 0.0786$, $m = 0.149$, and $n = 0.396$. For their data, the correlation had a mean

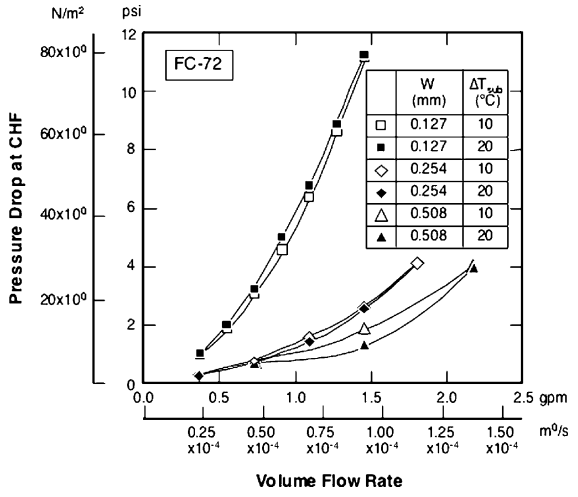

Fig. 9. Pressure drop at CHF for FC-72 versus flow rate for different jet widths and subcoolings.

absolute error of 7.4% and a maximum deviation of 18.2%.

Different attempts were made to correlate the present CHF data according to the dimensionless form of Eq. (8). Applying the original Mudawar and Wadsworth correlation to the present FC-72 data yielded a mean absolute error of 13.18%. To correct the correlation for multi-jet interactions and exit geometry, the length, L, was first replaced with a pseudo-surface length, $L - W_e$, where W_e is the total width of the exits for a single jet cell. This reduced the mean absolute error for FC-72 to 5.20%. However, optimum correlation of the present data was achieved by re-optimizing the empirical constants in Eq. (8). Fig. 10 shows the resulting correlation

$$q_m^{**} = \frac{\left[\frac{q''_m/(\rho_g h_{fg})}{U}\right]}{\left[\frac{\rho_f}{\rho_g}\right]^{2/3}\left[1+\frac{c_{pf}\Delta T_{sub}}{h_{fg}}\right]^{1/3}\left[1+0.034\frac{\rho_f c_{pf}\Delta T_{sub}}{\rho_g h_{fg}}\right]^{2/3}\left[\frac{W}{L-W}\right]^{0.331}} = 0.0919\left[\frac{\sigma}{\rho_f U^2 (L-W)}\right]^{0.157}, \tag{9}$$

fits the present data with a mean absolute error for FC-72 of 3.53%. Also included in Fig. 10 are seven CHF data points for ethanol. While these points show larger deviation than for FC-72, Eq. (9) provides an overall mean absolute error for both fluids of only 7.76%.

For $W \ll L$, Eq. (9) yields the following dependence of CHF on jet width and velocity:

$$q_m^{Prime} \propto U^{0.686} W^{0.331} = U^{0.355}(UW)^{0.331} = \frac{(UW)^{0.686}}{W^{0.355}}. \tag{10}$$

Eq. (10) implies a higher CHF can be achieved for a fixed flow rate simply by decreasing jet width.

5.2. Surface temperature variations at CHF

Since an isothermal surface is highly desirable in electronic cooling applications, it is useful to examine the temperature variations across the test surface. These variations were generally greatest at CHF.

The surface temperature variations at CHF for FC-72 are summarized in Table 3. Overall, the maximum temperature deviation for all tests was 2.6 °C, which occurred for two cases: (a) 0.127 mm jet at 8 m/s and 20.6 °C subcooling, and (b) 0.127 mm jet at 4 m/s and 10.6 °C subcooling. The smallest deviation in adjacent surface temperatures was 0.1 °C, which occurred with

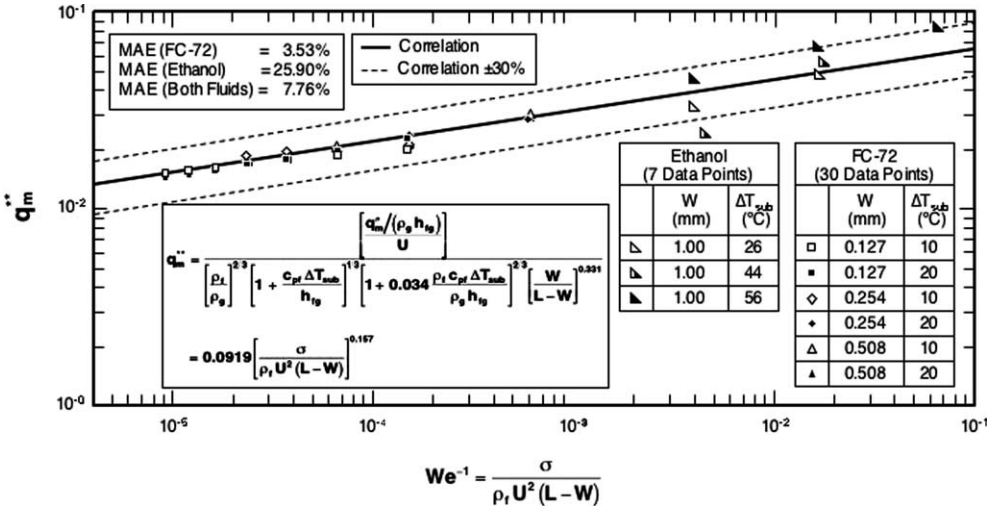

Fig. 10. Correlation of CHF data.

Table 3
Local surface temperatures at CHF for FC-72

W (mm)	U (m/s)	$\Delta T_{sub} = 10.6 \pm 0.3$°C				$\Delta T_{sub} = 20.6 \pm 0.3$ °C			
		T_1 (°C)	T_2 (°C)	T_3 (°C)	ΔT_{max} (°C)	T_1 (°C)	T_2 (°C)	T_3 (°C)	ΔT_{max} (°C)
0.508	1.0	95.0	97.1	95.6	2.1	89.8	91.8	90.3	1.0
	2.0	94.5	96.6	95.2	2.1	91.9	92.7	91.5	
	3.0	96.3	96.7	95.6		94.6	95.3	93.8	
0.254	1.0	90.5	91.1	90.2		86.5	87.0	86.2	
	2.0	86.6	88.1	86.8	1.5	84.6	85.9	84.6	
	3.0	87.2	88.2	88.1		86.7	88.3	86.9	1.6
	4.0	91.5	92.2	91.1		87.8	88.9	87.5	
	5.0	92.3	93.4	92.8		89.4	89.7	88.7	
0.127	2.0	86.3	88.2	86.8		91.3	93.1	91.3	
	3.0	92.7	94.5	93.0		91.7	93.9	92.0	
	4.0	92.9	94.8	93.0		90.7	93.3	91.2	2.6
	5.0	94.3	96.5	94.6		92.8	94.2	92.4	
	6.0	94.7	96.9	94.9		92.0	93.4	91.6	
	7.0	96.5	98.7	96.7		92.4	93.8	92.1	
	8.0	94.3	96.9	94.9	2.6	92.1	93.7	91.6	

T_1: Temperature under outside jet.
T_2: Temperature between jets.
T_3: Temperature under center jet.
ΔT_{max}: Largest difference between three surface temperatures for given width and subcooling.

the 0.254 mm jet at 3 m/s and 10.6 °C subcooling. Overall, the largest surface temperature variations were encountered with the 0.127 mm jets, which had an average difference of 1.9 °C between adjacent surface temperatures. The average differences for the 0.254 and 0.508 mm jets were 1.0 and 1.4 °C, respectively. While these numbers do not suggest a definitive trend for surface temperature variations with jet width, they do prove the present cooling configuration is highly effective at maintaining fairly isothermal surface temperatures.

6. Conclusions

This study explored the heat transfer characteristics of an array of FC-72 and ethanol rectangular jets that were used to cool a 3.0 cm × 3.0 cm surface. The effects of jet velocity, jet width and subcooling were examined to construct new correlations for both the single-phase heat transfer coefficient and CHF, and to assess such practical considerations as flow rate and pressure drop requirements, and the ability to ensure fairly isothermal surface conditions. Key findings from the study are as follows:

(1) The single-phase heat transfer coefficient for FC-72 increases with increases in impingement velocity and/or jet width. A correlation for single-phase cooling is constructed by dividing a unit jet cell into an impingement zone and two confinement channel regions that are dominated by wall jet flow. This correlation method is highly effective at correlating the present single-phase data, evidenced by a mean absolute error of 2.96%.
(2) Increases in jet velocity, jet width, and/or subcooling broaden the single-phase region preceding the commencement of boiling. Within the nucleate boiling region, data for different jet widths and velocities for a given subcooling tend to converge.
(3) CHF increases with increases in jet velocity and/or jet width. CHF is also significantly enhanced by increasing the inlet subcooling. For the range of velocities examined, an additional 10 °C of subcooling increases CHF for FC-72 on average by 18 W/cm^2 or 26%. A new CHF correlation that accounts for fluid properties, jet velocity, nozzle width, and subcooling was developed which fits the experimental data with a mean absolute error of 7.76%.
(4) Better cooling performance is realized for a given flow rate by decreasing jet width. Pressure drop is for the most part quite modest, even for the smallest jet width and highest velocity tested. Overall, the present cooling scheme is highly effective at dissipating in excess of 100 W/cm^2 and maintaining fairly isothermal surface conditions with spatial variations of less than 1.2 and 2.6 °C for the single-phase and boiling regions, respectively.

Acknowledgements

The authors are grateful for the support of Raytheon Company, Tucson, AZ.

References

[1] I. Mudawar, Assessment of high-heat-flux thermal management schemes, IEEE Trans.–Compon. Pack. Tech. 24 (2001) 122–141.
[2] M. Monde, T. Inoue, Critical heat flux in saturated forced convection boiling on a heated disk with multiple jets, ASME J. Heat Transfer 113 (1991) 722–727.
[3] Y. Katto, M. Monde, 1974, Study of mechanism of burnout in high heat flux boiling systems with an impinging jet, in: Proc. 5th Int. Heat Transfer Conf., Tokyo, Japan (1974), pp. 245–249.
[4] M. Monde, Y. Katto, Burnout in high heat-flux boiling system with an impinging jet, Int. J. Heat Mass Transfer 21 (1978) 295–305.
[5] Y. Kato, M. Shimizu, Upper limit of CHF in the saturated forced convection boiling system with an impinging jet, ASME J. Heat Transfer 101 (1979) 265–269.
[6] M. Monde, Critical heat flux in saturated forced convection boiling on a heated disk with an impinging jet, ASME J. Heat Transfer 109 (1987) 991–996.
[7] K.A. Estes, I. Mudawar, Comparison of two-phase electronic cooling using free jets and sprays, ASME J. Electron. Pack. 117 (1995) 323–332.
[8] M.E. Johns, I. Mudawar, An ultra-high power two-phase jet-impingement avionic clamshell module, ASME J. Electron. Pack. 118 (1996) 264–270.
[9] D.C. Wadsworth, I. Mudawar, Enhancement of single-phase heat transfer and critical heat flux from an ultra-high-flux simulated microelectronic heat source to a rectangular impinging jet of dielectric liquid, ASME J. Heat Transfer 114 (1992) 764–768.
[10] I. Mudawar, D.C. Wadsworth, Critical heat flux from a simulated chip to a confined rectangular impinging jet of dielectric liquid, Int. J. Heat Mass Transfer 34 (1991) 1465–1479.
[11] E.U. Schlunder, P. Krotzsch, F.W. Hennecke, Gresetzmaßigkeiten der warme-und stoffubertragung bei der prallstromung aus rund-und schlitzdusen, Chem. Ingenieur Tech. 42 (1970) 333–338.
[12] H. Martin, Heat and mass transfer between impinging gas jets and solid surfacesAdvances in Heat Transfer, 13, Academic Press, New York, NY, 1977, pp. 1–60.